Journal of Applied Physics

Micro-machined deep silicon atomic vapor cells

Cite as: J. Appl. Phys. **132**, 134401 (2022); https://doi.org/10.1063/5.0114762
Submitted: 26 July 2022 • Accepted: 07 September 2022 • Published Online: 03 October 2022
Published open access through an agreement with JISC Collections

S. Dyer, P. F. Griffin, A. S. Arnold, et al.

ARTICLES YOU MAY BE INTERESTED IN

Micro-fabricated components for cold atom sensors
Review of Scientific Instruments **93**, 091101 (2022); https://doi.org/10.1063/5.0101628

Dependence of the radiative lifetime on the type-II band offset in $GaAs_xSb_{1-x}/GaAs$ quantum dots including effects of photoexcited carriers
Journal of Applied Physics **132**, 134402 (2022); https://doi.org/10.1063/5.0105306

Thickness-scaling phonon resonance: A systematic study of hexagonal boron nitride from monolayers to bulk crystals
Journal of Applied Physics **132**, 134302 (2022); https://doi.org/10.1063/5.0094039

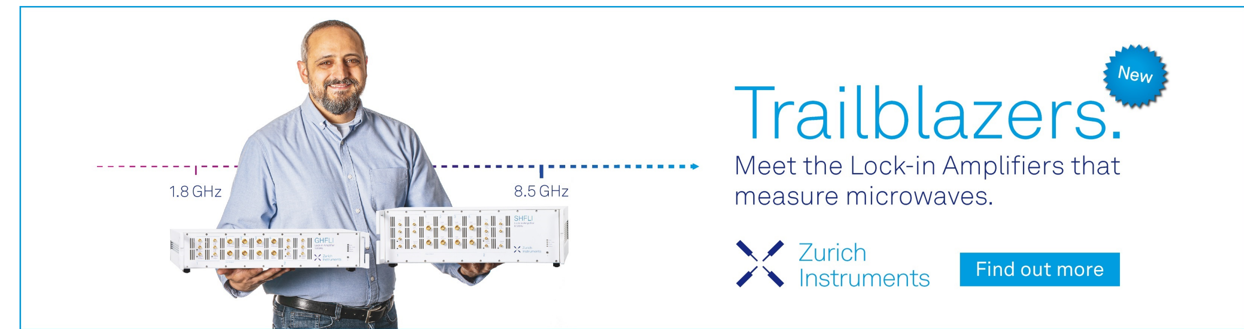

© 2022 Author(s).

Micro-machined deep silicon atomic vapor cells

Cite as: J. Appl. Phys. **132**, 134401 (2022); doi: 10.1063/5.0114762
Submitted: 26 July 2022 · Accepted: 7 September 2022 ·
Published Online: 3 October 2022

S. Dyer,[1] P. F. Griffin,[1] A. S. Arnold,[1] F. Mirando,[2] D. P. Burt,[2] E. Riis,[1] and J. P. McGilligan[1,a)]

AFFILIATIONS

[1]Department of Physics, SUPA, University of Strathclyde, Glasgow G4 0NG, United Kingdom
[2]Kelvin Nanotechnology, University of Glasgow, Glasgow G12 8LS, United Kingdom

[a)]**Author to whom correspondence should be addressed:** james.mcgilligan@strath.ac.uk

ABSTRACT

Using a simple and cost-effective water jet process, silicon etch depth limitations are overcome to realize a 6 mm deep atomic vapor cell. While the minimum silicon feature size was limited to a 1.5 mm width in these first generation vapor cells, we successfully demonstrate a two-chamber geometry by including a ∼25 mm meandering channel between the alkali pill chamber and the main interrogation chamber. We evaluate the impact of the channel conductance on the introduction of the alkali vapor density during the pill activation process and mitigate glass damage and pill contamination near the main chamber. Finally, we highlight the improved signal achievable in the 6 mm silicon cell compared to standard 2 mm path length silicon vapor cells.

© 2022 Author(s). All article content, except where otherwise noted, is licensed under a Creative Commons Attribution (CC BY) license (http://creativecommons.org/licenses/by/4.0/). https://doi.org/10.1063/5.0114762

I. INTRODUCTION

The micro-fabrication of atomic sensors has enabled a revolution in the field deployment and commercialization of chip-scale atomic sensors.[1–4] A critical component at the core of many of these chip-scale devices is the atomic vapor cell, consisting typically of a micro-electro-mechanical system (MEMS) based glass–silicon–glass stack bonded under vacuum.[5] Such MEMS cells have been widely explored for compact sensors, forming hermetic seals from both anodic and thermo-compression bonds to provide a mass-producible cell manufacturing solution.[5–7] While this now mature technology has enabled the transition to miniature components for atomic sensors, the methods of manufacturing silicon have typically limited the available optical path length to around 2 mm. These limitations arise due to dry etch phenomena[8] and challenges associated with long duration wet etch processes.[9] However, a longer optical path length would be beneficial for atomic sensors due to the increased atomic absorption and the associated enhancement in the signal-to-noise ratio. With this in mind, alternative techniques have been explored to increase the optical path length in line-of-sight cells, such as the mechanical drilling of 4 mm thick glass body cells[10] or the ultrasonic drilling of 4 mm thick silicon frames.[11]

To circumvent the short line-of-sight path length available in conventional micro-fabricated cells, alternative light routing methods have been explored. A notable example is a wet-etched elongated silicon cell, with reflective walls at 54.7° from the wafer surface that direct the incident light through the long axis of the silicon cell, to achieve an optical path length of 7 mm.[12] However, the additional complexity required to achieve optically smooth walls, as well as the inclusion of glass-etched grating structures, critically aligned to manipulate the angle of incidence for light routing parallel to the silicon surface, make this process costly and complex. While novel approaches to light routing in silicon cells may enable an increased optical path length,[13,14] the benefits of simple deep line-of-sight cells would also be valuable for chip-scale laser cooling, where the 6 mm silicon thickness could enable a larger optical overlap volume within the cell.[15]

Recent investigations of laser cooling in MEMS cells have reported a degradation of the achievable trapped atom number due to a limited silicon frame thickness, which restricts the optical overlap volume within the cell.[15] A viable solution for both hot and cold atom MEMS cells would be an increased optical path length in line-of-sight cells.

Here, we introduce a micro-machined silicon-based vapor cell, manufactured with water jet cutting to achieve an optical path length of 6 mm in a simple line-of-sight geometry. An alkali pill deposited in the silicon frame provides a natural Rb density within the cell, with a meandering channel used to reduce material spray and permanent discoloration of glass in the main chamber of the cell. The step-change from conventional semiconductor fabrication processes to micro-machining for silicon-based vapor cell

production greatly reduces the manufacturing costs by mitigating the need for photolithography and etching processes, while providing an improved optical path length to greatly increase the capabilities of chip-scale atomic sensors.

II. FABRICATION AND SETUP

The silicon frame of the cell is manufactured using a high pressure water jet cutting process. While this method is not limited to the depth restrictions placed upon micro-fabricated silicon, the minimum feature size is degraded. In this first generation cell, a minimum feature width of 1.5 mm was realized for the conductance channel between the pill source and the main interrogation chamber. Non-line-of-sight conductance channels have been shown to be critical in reducing material spray and glass discoloration in the interrogation region of the vapor cell.[7,16,17] Previously, non-line-of-sight channels have been dry etched with feature sizes on the order of $200 \times 200\,\mu m^2$ to greatly reduce the conductance into the main chamber, while permitting the presence of a suitable vapor density.[16] Since the micro-machined channel's cross-sectional area is $\sim \times 220$ larger than conventional dry etched channels,[16] a long meandering path was machined between the pill location and the main chamber, as shown in Fig. 1(a). The main cubic chamber was fabricated with dimensions $(6\,\text{mm})^3$ to enable wider beams to be used for an improved signal-to-noise ratio in atomic spectroscopy.

During water jet cutting, no protective layer was used to cover the bonding surface. As a result, chipping of the silicon was observed around the perimeters of the cut regions, with features on the order of $100\,\mu m$. However, these small defects did not hinder the hermetic sealing of the cell. Additionally, some preliminary measurements have shown that this can be mitigated by wax adhering glass wafers to both bonding surfaces prior to the water jet process.

Following the water jet cutting, the silicon wafers are solvent cleaned in an ultra-sonic bath. After the cleaning stage, the silicon inner wall surface roughness was evaluated with surface profilometry and scanning electron microscopy (SEM). SEM images shown in Figs. 1(b) and 1(c) were used to qualitatively evaluate the potential impact of wall roughness on the atomic vapor cell; an increased surface area could consume more alkali content and hinder the homogeneity of applied wall coatings that may be required in later applications. The surface profilometry measurements determined an arithmetic average wall roughness of $R_a = 5.9\,\mu m$. While this wall roughness is comparable to recent work in additively manufactured vacuum chambers,[18] it remains orders of magnitude larger than the wall roughness achievable for deep reactive-ion etching (DRIE), with short etch depths ($\leq 100\,\mu m$) achieving $R_a = 5$ nm[8,19] and deep etched silicon (1.4 mm) demonstrating $R_a = 300$ nm.[20] In future applications, chemical smoothing of the inner walls can be applied if the wall roughness is found to hinder the atomic vapor cell's long-term performance.[20]

Following manufacturing, the silicon wafer was anodically bonded to 0.5 mm thick borosilicate glass wafers at both interfaces in a total background pressure of $\approx 10^{-5}$ mbar. Prior to bonding, a commercially available alkali pill dispenser (SAES Rb/AMAX/Pill1-0.6) was deposited in the dedicated pill chamber of the silicon frame. The alkali pill was selected as the atomic source due to the relatively low background gas contamination compared to azide and chloride compounds,[21] enabling applications in wavelength referencing.[22,23] Post bonding, the wafer stack was diced into cells with total dimensions measuring $13 \times 13 \times 7\,\text{mm}^3$ (L × W × H). To control the alkali vapor pressure, surface mounted resistors adhered to the front and back glass surfaces were used to heat the cell. The steady-state cell temperature was measured with a thermal camera.

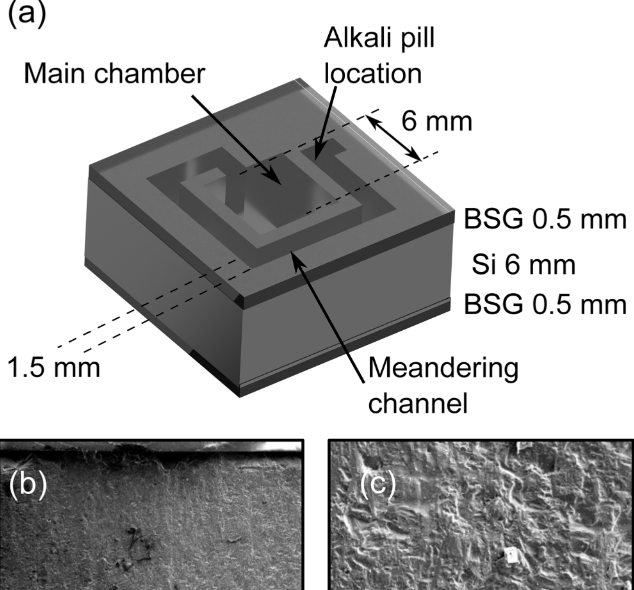

FIG. 1. (a) Illustration of the micro-machined silicon vapor cell. The cell is composed of a borosilicate glass (BSG)–Si–BSG stack, with total outer dimensions of $(13\,\text{mm})^2 \times 7$ mm. The main cubic chamber has a $(6\,\text{mm})^3$ volume, connected to an alkali micro-pill dispenser via a meandering channel with a cross-sectional area of $1.5 \times 6\,\text{mm}^2$. (b) and (c) Scanning electron microscope (SEM) images of the micro-machined silicon surface.

A Yb fiber laser at 1070 nm was used for pill activation and focused to fill the pill surface. A digital single-lens reflex camera was used to extract images of the cell window damage over time during the pill activation. A volume Bragg-reflector (VBR) laser at 780 nm was fiber-coupled and aligned through a polarizing beam-splitter (PBS) and the main chamber of the MEMS cell. The light was retro-reflected for *in situ* "saturated absorption spectroscopy,"[24] with the photodiode using a 780 ± 2 nm bandpass filter to avoid saturation from the Yb fiber laser during activation.

III. RESULTS

The alkali pill source in each individual cell was laser heated[25] for 10 s with 3 W of 1070 nm light, focused to fill the 1 mm

© Author(s) 2022

diameter of the pill surface. The activation process and subsequent material diffusion are highlighted in Figs. 2(a)–2(f). In this demonstration, the cell was heated to 60 °C to drive alkali diffusion through the channel and into the main chamber. Images of a cell with no channel present during activation are shown in Figs. 2(g)–2(i). The peak absorption evolution of the D_2 ^{85}Rb $F = 3$ ground state was simultaneously measured [Fig. 2(j)] from *in situ* saturated absorption spectroscopy during the activation process of both cell types. For these measurements, the laser intensity was 1.6 mW/cm^2.

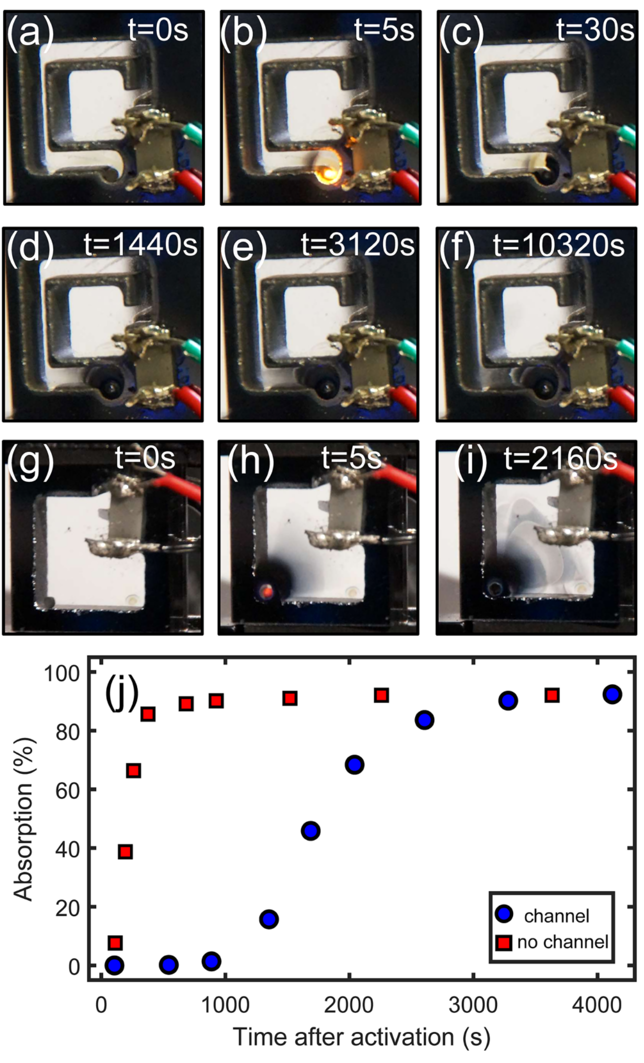

FIG. 2. Activation process of the alkali pill with laser heating: prior to activation (a); during the 10 s activation with 3 W of 1070 nm light (b); immediately after activation, where glass damage can be seen, as well as the presence of Rb on the glass surfaces (c). The migration of pill released material after activation was then observed (d)–(f). Images (g)–(i) show a cell with no serpentine channel before, during, and after activation, respectively. (j) Simultaneously measured strongest D_2 transition absorption from the ^{85}Rb $F = 3$ ground state in the main chamber during the activation process for a channel and no-channel cell.

The cell prior to pill activation is seen at $t = 0$ s in Fig. 2(a), followed by a 10 s pulse of laser heating with 3 W of 1070 nm light [shown at $t = 5$ s in Fig. 2(b)]. While it is noted that the pill could be activated with lower laser powers, the chosen parameters ensured a reproducible activation between the cells under test. In the short time following activation, darkening of the glass is observed around the activation site, which progressively migrates through the conductance channel between $t = 30$ and 10 320 s. Simultaneously, a silver spray of an Rb metal can be seen migrating through the channel, with the growth of atomic absorption plateauing in the main chamber after $t \sim 3000$ s. Additionally, an identical cell was activated without heating during pill activation. In this scenario, Rb is accumulated near the pill activation site on the rough walls created by the mechanical micro-machining of the silicon frame. This was overcome by subsequent heating of the cell to again encourage migration into the main chamber.

In contrast, a comparable cell without the meandering channel was fabricated, activated, and observed in a similar manner [Figs. 2(g)–2(i)]. The absence of the channel between the pill and the interrogation cell results in the activation process spraying material across the glass and reducing the cell optical access. Simultaneously, the absorption within the cell saturates much earlier at $t \sim 400$ s, as there is no diffusion time constant associated with reaching the cell interrogation region.

Following the activation process and measurement of the alkali vapor density within the main cell, the cell absorption spectra were analyzed, as shown in Fig. 3. The spectrum provided

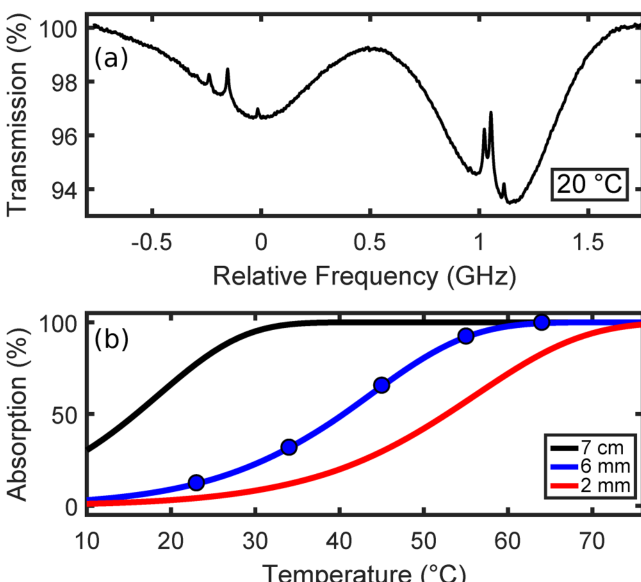

FIG. 3. (a) Typical D_2 line saturated absorption spectrum (single-shot) for the 6 mm meandering micro-machined cell at room temperature. (b) Peak absorption from the ^{85}Rb $F = 3$ ground state Doppler-broadened profile as a function of temperature for retro-reflected vapor cells of 7 cm (black), 6 mm (blue), and 2 mm (red) path lengths. Blue data points represent measurements taken with the meandering 6 mm vapor cell.

© Author(s) 2022

in Fig. 3(a) was obtained using a beam waist of ~2 mm (1/e^2 radius) and a peak intensity of 5 mW/cm^2. For this room temperature measurement, ≈7.5% peak D_2 absorption was measured from the ^{85}Rb $F = 3$ ground states. It is noted that the linewidth of the sub-Doppler features is $\sim \times 1.4$ broader than comparable measurements in a glass reference cell over a range of incident intensities. While the cause of the broadening remains under investigation, the observation of similar broadening in other pill based MEMS cells indicates that the cause could be from non-Rb content released during pill activation.

Figure 3(b) illustrates the peak absorption of the ^{85}Rb $F = 3$ ground state as a function of the measured cell temperature. The blue data points and curve show the measured and theoretically expected absorption at various temperatures for a 6 mm cell length, respectively.[26] The 6 mm cell data are compared to theoretical curves for a typical 7 cm long glass blown cell (black) and a 2 mm path length micro-fabricated cell (red). For these measurements, a beam waist of ~ 2 mm and a peak intensity of 0.2 mW/cm^2 were used. We observed good correlation between experimental and theoretical absorption. For an operation temperature of 47 °C, the 6 mm cell is capable of achieving the same absorption level as a room temperature 7 cm cell, while the 2 mm cell would require heating to 60 °C. Additionally, the optical path length of the deep silicon machined frame provides a sufficient signal-to-noise ratio for laser stabilization to the atomic reference cell at room temperature.

In future work, we will evaluate the performance of the deep micro-machined cell as a wavelength reference for laser locking in a chip-scale laser cooling system. Additionally, the ability to fabricate 6 mm thick MEMS cells is directly transferable to the development of ultrahigh-vacuum MEMS cells, where the increased vacuum volume would benefit the achievable optical overlap volume and the trapped atom number.[15,27,28]

IV. CONCLUSION

We have demonstrated the suitability of deep micro-machined silicon frames for the production of MEMS atomic vapor cells. While the first demonstration has a silicon feature width limitation of 1.5 mm, the inclusion of a meandering channel has been demonstrated to sufficiently restrict unwanted glass discoloration from the pill activation process outside of the main chamber for unhindered optical interrogation. The increased optical path length was demonstrated in saturated absorption spectroscopy, with an atomic absorption significantly larger than is achievable in standard 2 mm MEMS vapor cells. The manufacturing simplicity and cost reduction of this technique make this a highly attractive route for macro-scale cell fabrication in atomic sensors where increased optical path lengths are desired.

ACKNOWLEDGMENTS

The authors would like to thank R. Boudot for useful conversations and careful reading of the manuscript. Additionally, we thank B. Lewis and A. Bregazzi for their reading of the manuscript. The authors acknowledge funding from Innovate UK (Project No. 50133). J.P.M. gratefully acknowledges funding from the Royal Academy of Engineering Research Fellowship.

AUTHOR DECLARATIONS

Conflict of Interest

The authors have no conflicts to disclose.

Author Contributions

S. Dyer: Conceptualization (equal); Data curation (equal); Formal analysis (equal); Investigation (equal); Methodology (equal); Software (equal); Validation (equal); Visualization (equal); Writing – original draft (equal); Writing – review & editing (equal). **P. F. Griffin:** Formal analysis (equal); Funding acquisition (equal); Supervision (supporting); Validation (supporting); Writing – original draft (supporting); Writing – review & editing (supporting). **A. S. Arnold:** Formal analysis (supporting); Funding acquisition (equal); Methodology (supporting); Software (equal); Supervision (supporting); Visualization (supporting); Writing – original draft (supporting); Writing – review & editing (supporting). **F. Mirando:** Conceptualization (supporting); Data curation (supporting); Investigation (supporting); Resources (equal); Software (equal); Visualization (equal); Writing – original draft (supporting); Writing – review & editing (supporting). **D. P. Burt:** Conceptualization (supporting); Data curation (supporting); Formal analysis (supporting); Funding acquisition (equal); Investigation (supporting); Methodology (supporting); Project administration (supporting); Resources (equal); Software (equal); Supervision (supporting); Validation (supporting); Visualization (supporting); Writing – original draft (supporting); Writing – review & editing (supporting). **E. Riis:** Conceptualization (supporting); Data curation (supporting); Formal analysis (supporting); Funding acquisition (equal); Investigation (supporting); Methodology (supporting); Project administration (supporting); Resources (equal); Supervision (equal); Validation (equal); Visualization (supporting); Writing – original draft (supporting); Writing – review & editing (supporting). **J. P. McGilligan:** Conceptualization (lead); Data curation (lead); Formal analysis (equal); Funding acquisition (supporting); Investigation (lead); Methodology (lead); Project administration (lead); Resources (equal); Software (equal); Supervision (equal); Validation (lead); Visualization (lead); Writing – original draft (lead); Writing – review & editing (lead).

DATA AVAILABILITY

The data that support the findings of this study are available from the corresponding author upon reasonable request.

REFERENCES

[1] S. Knappe, V. Shah, P. D. D. Schwindt, L. Hollberg, J. Kitching, L.-A. Liew, and J. Moreland, "A microfabricated atomic clock," Appl. Phys. Lett. **85**, 1460–1462 (2004).

[2] R. Vicarini, M. Abdel Hafiz, V. Maurice, N. Passilly, E. Kroemer, L. Ribetto, V. Gaff, C. Gorecki, S. Galliou, and R. Boudot, "Mitigation of temperature-induced light-shift effects in miniaturized atomic clocks," IEEE Trans. Ultrason. Ferroelectr. Freq. Control **66**, 1962–1967 (2019).

[3] D. Hunter, R. Jiménez-Martínez, J. Herbsommer, S. Ramaswamy, W. Li, and E. Riis, "Waveform reconstruction with a Cs based free-induction-decay magnetometer," Opt. Express **26**, 30523–30531 (2018).

© Author(s) 2022

[4]V. Shah, S. Knappe, P. D. D. Schwindt, and J. Kitching, "Subpicotesla atomic magnetometry with a microfabricated vapour cell," Nat. Photonics **1**, 649–652 (2007).
[5]L.-A. Liew, S. Knappe, J. Moreland, H. Robinson, L. Hollberg, and J. Kitching, "Microfabricated alkali atom vapor cells," Appl. Phys. Lett. **84**, 2694–2696 (2004).
[6]J. Kitching, "Chip-scale atomic devices," Appl. Phys. Rev. **5**, 031302 (2018).
[7]S. Karlen, J. Haesler, T. Overstolz, G. Bergonzi, and S. Lecomte, "Sealing of MEMS atomic vapor cells using Cu-Cu thermocompression bonding," J. Microelectromech. Syst. **29**, 95–99 (2020).
[8]F. Laermer, S. Franssila, L. Sainiemi, and K. Kolari, "Deep reactive ion etching," in *Handbook of Silicon Based MEMS Materials and Technologies*, Micro and Nano Technologies, 3rd ed., edited by M. Tilli, M. Paulasto-Krockel, M. Petzold, H. Theuss, T. Motooka, and V. Lindroos (Elsevier, 2020), Chap. 16, pp. 417–446.
[9]J. P. McGilligan, K. F. Gallacher, P. F. Griffin, D. J. Paul, A. S. Arnold, and E. Riis, "Invited review: Micro-fabricated components for cold atom sensors," Rev. Sci. Instr. (to be published) (2022).
[10]Y. Pétremand, C. Affolderbach, R. Straessle, M. Pellaton, D. Briand, G. Mileti, and N. F. de Rooij, "Microfabricated rubidium vapour cell with a thick glass core for small-scale atomic clock applications," J. Micromech. Microeng. **22**, 025013 (2012).
[11]S. Woetzel, V. Schultze, R. IJsselsteijn, T. Schulz, S. Anders, R. Stolz, and H.-G. Meyer, "Microfabricated atomic vapor cell arrays for magnetic field measurements," Rev. Sci. Instrum. **82**, 033111 (2011).
[12]R. Chutani, V. Maurice, N. Passilly, C. Gorecki, R. Boudot, M. Abdel Hafiz, P. Abbé, S. Galliou, J.-Y. Rauch, and E. de Clercq, "Laser light routing in an elongated micromachined vapor cell with diffraction gratings for atomic clock applications," Sci. Rep. **5**, 14001 (2015).
[13]H. Nishino, Y. Furuya, and T. Ono, "Micro-fabricated vapor cells with sealed Rb atoms by distillation at wafer level and two-step bonding for miniature atomic clocks," Opt. Express **29**, 44316–44321 (2021).
[14]H. Nishino, M. Hara, Y. Yano, M. Toda, Y. Kanamori, M. Kajita, T. Ido, and T. Ono, "A reflection-type vapor cell using anisotropic etching of silicon for micro atomic clocks," Appl. Phys. Express **12**, 072012 (2019).
[15]A. Bregazzi, P. F. Griffin, A. S. Arnold, D. P. Burt, G. Martinez, R. Boudot, J. Kitching, E. Riis, and J. P. McGilligan, "A simple imaging solution for chip-scale laser cooling," Appl. Phys. Lett. **119**, 184002 (2021).
[16]Z. L. Newman, V. Maurice, T. Drake, J. R. Stone, T. C. Briles, D. T. Spencer, C. Fredrick, Q. Li, D. Westly, B. R. Ilic, B. Shen, M.-G. Suh, K. Y. Yang, C. Johnson, D. M. S. Johnson, L. Hollberg, K. J. Vahala, K. Srinivasan, S. A. Diddams, J. Kitching, S. B. Papp, and M. T. Hummon, "Architecture for the photonic integration of an optical atomic clock," Optica **6**, 680–685 (2019).
[17]V. Maurice, J. Rutkowski, E. Kroemer, S. Bargiel, N. Passilly, R. Boudot, R. Chutani, S. Galliou, C. Gorecki, L. Mauri, and M. Moraja, "Microfabricated vapor cells for miniature atomic clocks based on post-sealing activated cesium dispensers," in *2017 Joint Conference of the European Frequency and Time Forum and IEEE International Frequency Control Symposium (EFTF/IFCS)* (IEEE, 2017), pp. 636–637.
[18]N. Cooper, L. Coles, S. Everton, I. Maskery, R. Campion, S. Madkhaly, C. Morley, J. O'Shea, W. Evans, R. Saint, P. Krüger, F. Oručević, C. Tuck, R. Wildman, T. Fromhold, and L. Hackermüller, "Additively manufactured ultra-high vacuum chamber for portable quantum technologies," Addit. Manuf. **40**, 101898 (2021).
[19]K.-S. Chen, A. Ayon, X. Zhang, and S. Spearing, "Effect of process parameters on the surface morphology and mechanical performance of silicon structures after deep reactive ion etching (DRIE)," J. Microelectromech. Syst. **11**, 264–275 (2002).
[20]R. Chutani, M. Hasegawa, V. Maurice, N. Passilly, and C. Gorecki, "Single-step deep reactive ion etching of ultra-deep silicon cavities with smooth sidewalls," Sens. Actuators, A **208**, 66–72 (2014).
[21]D. G. Bopp, V. M. Maurice, and J. E. Kitching, "Wafer-level fabrication of alkali vapor cells using in-situ atomic deposition," J. Phys.: Photonics **3**, 015002 (2020).
[22]A. Douahi, L. Nieradko, J. Beugnot, J. Dziuban, H. Maillote, R. Boudot, S. Guerandel, M. Moraja, C. Gorecki, and V. Giordano, "New vapor cell technology for chip scale atomic clock," in *2007 IEEE International Frequency Control Symposium Joint with the 21st European Frequency and Time Forum* (IEEE, 2007), pp. 58–61.
[23]Z. L. Newman, V. Maurice, C. Fredrick, T. Fortier, H. Leopardi, L. Hollberg, S. A. Diddams, J. Kitching, and M. T. Hummon, "High-performance, compact optical standard," Opt. Lett. **46**, 4702–4705 (2021).
[24]D. A. Smith and I. G. Hughes, "The role of hyperfine pumping in multilevel systems exhibiting saturated absorption," Am. J. Phys. **72**, 631–637 (2004).
[25]P. F. Griffin, K. J. Weatherill, and C. S. Adams, "Fast switching of alkali atom dispensers using laser-induced heating," Rev. Sci. Instrum. **76**, 093102 (2005).
[26]P. Siddons, C. S. Adams, C. Ge, and I. G. Hughes, "Absolute absorption on rubidium D lines: Comparison between theory and experiment," J. Phys. B **41**, 155004 (2008).
[27]J. P. McGilligan, K. R. Moore, A. Dellis, G. D. Martinez, E. de Clercq, P. F. Griffin, A. S. Arnold, E. Riis, R. Boudot, and J. Kitching, "Laser cooling in a chip-scale platform," Appl. Phys. Lett. **117**, 054001 (2020).
[28]A. Bregazzi, S. Dyer, P. F. Griffin, D. P. Burt, A. S. Arnold, E. Riis, and J. P. McGilligan, Enabling the mass production of a chip-scale laser cooling platform," Proc. SPIE **11881**, 100–110 (2021).

© Author(s) 2022